

We are IntechOpen, the world's leading publisher of Open Access books Built by scientists, for scientists

6,900

Open access books available

186,000

International authors and editors

200M

Downloads

Our authors are among the

154

Countries delivered to

TOP 1%

most cited scientists

12.2%

Contributors from top 500 universities



WEB OF SCIENCE™

Selection of our books indexed in the Book Citation Index
in Web of Science™ Core Collection (BKCI)

Interested in publishing with us?
Contact book.department@intechopen.com

Numbers displayed above are based on latest data collected.
For more information visit www.intechopen.com



Improved Performance of a Photovoltaic Panel by MPPT Algorithms

Djamel Eddine Tourqui, Achour Betka,
Atallah Smaili and Tayeb Allaoui

Additional information is available at the end of the chapter

<http://dx.doi.org/10.5772/intechopen.79709>

Abstract

This work is devoted to the presentation and realization of a digital control card (maximum power point tracking) which serves to improve the performance of a photovoltaic generator (GPV). This makes it possible to increase the profitability of the latter, on the one hand, and the stability of electrical networks, on the other hand. The command card has been developed using simple circuits, and tested on a system that includes a photovoltaic panel powering a resistive load under changing weather conditions. The aim of this paper is to implement three well-known MPPT algorithms (Hill-Climbing, Pertube & Observe and Incremental Conductance), using a PIC microcontroller type 16F877A.

Keywords: photovoltaic panel, MPPT, PIC 16F877A, P&O, Hill-climbing, incremental conductance

1. Introduction

Solar energy is among the most widely used sources of renewable energy on a global scale with an installed global capacity of up to 100 GW [1]. This source is considered one of the most promising and best alternative energy source because of its natural availability and cleanliness [2, 3].

It is known that photovoltaic panels have a non-linear characteristic $I = f(V)$ with a single point where the power generated is maximum (PPM). It is known that PV panels have a non-linear characteristic $I = f(V)$ with a single point where the power generated is maximum (MPP). This maximum power strongly depends on the intensity of solar radiation and the temperature, which changes during the day.

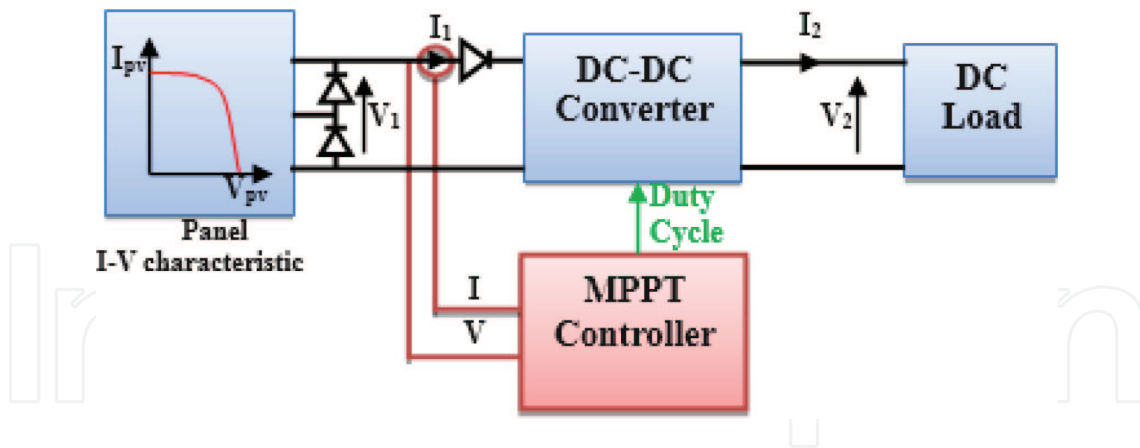


Figure 1. Elementary components of a PV power system.

However, the most difficulties associated with the use of a photovoltaic panel is the perfect non-coupling between the GPV photovoltaic generator and the load [4]. In direct connection mode, a technological barrier that exists in this type of coupling is the problem of transferring the maximum power of the GPV to the load, which often suffers from a bad adaptation. The resulting point of exploitation is then sometimes very far from the real MPP. In other words, it becomes difficult under these conditions to extract the maximum output power of PV panel in all weather conditions [5]. In order to extract at all times the maximum power available at the GPV terminals and transfer it to the load, an MPPT strategy is necessary in order to pursue the maximum power point of the PV panel [6]. There have been many research methods in the literature ranging from the simplest method like Disrupt & Observer (P & O) and IncCond to more sophisticated and complex [7–9].

Static converters, adapted to solar photovoltaic energy, are often called “solar converters” [10]. This adaptation can be achieved by inserting a series chopper controlled by a tracking mechanism “maximum power point tracking” (MPPT). **Figure 1** represents an elementary photovoltaic conversion elementary chain associated with an MPPT control.

2. Modeling of a photovoltaic generator

Figure 2 shows the equivalent electrical circuit (single-diode model) of a photovoltaic generator, which is used to calculate the power supplied by this generator under all irradiation and temperature conditions [11].

The relationship between the cell terminal current I and voltage V is given by [12, 13]:

$$I = I_{ph} - I_D \left[\exp \left(\frac{V + R_s \times I}{\frac{m \times K_B \times T_{amb}}{q}} \right) - 1 \right] - \frac{V + R_s \times I}{R_{sh}} \quad (1)$$

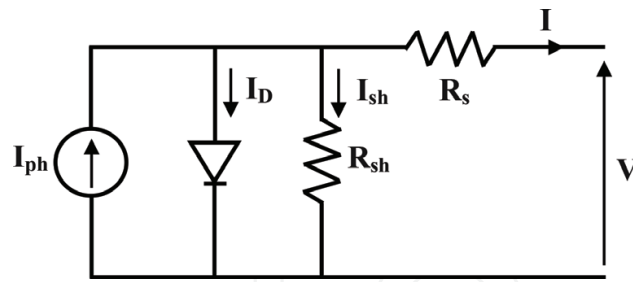


Figure 2. Equivalent circuit of the PV generator.

With:

I: output current, **I_D**: reverse saturation diode current, **I_{ph}** photovoltaic current, **KB**: Boltzmann constant ($1.3854 \times 10^{-23} \text{ JK}^{-1}$), **m**: ideality factor, **q**: Charge of an electron ($1.6021 \times 10^{-19} \text{ C}$), **R_s**: the series resistance (Ω) and **R_{sh}**: the shunt resistance (Ω).

As mentioned previously, the characteristic $I = f(V)$ (Figure 1) of a solar cell strongly depends on the illumination (**E**) and the ambient temperature (**T_{amb}**) [14]. The empirical model developed by Garcia and Balenzatgui gives the mathematical relation of the temperature of the photovoltaic module as follows [11, 15]:

$$T_m = T_{amb} + \frac{(\text{NOCT} - 20)E}{800} \quad (2)$$

In order to calculate the solar generator power (**P**), we used the model developed by Skoplaki and Palyvos [14] as follows:

$$P = E \times A \times \eta_{Tref} \left(1 - B_{ref} (T_m - 25) \right) \quad (3)$$

3. Overview of MPPT algorithms used

In the literature, there are various examples of MPPT technologies that serve to improve [8, 16, 17]. The Hill-Climbing, IncCond and Perturbe & Observe techniques are the most widely used because of their simplicity and ease of implementation. The operating principle of these three techniques is briefly summarized below:

3.1. Perturb and observe (P&O)

The principle of the P&O type MPPT commands consists in disturbing the panel voltage (V_{PV}) of a small amplitude around its initial value and analyzing the behavior of the instantaneous power variation P_{PV} of the photovoltaic panel before and after the disturbance [16, 18, 19]. If the change in dP_{PV} power increases, this implies that V_{PV} should be set in the same direction as in the previous cycle. If the power of dP_{PV} decreases, it means that the system is far from the optimal point, so the disturbance size must be reduced in order to bring the operating point around to

the point of maximum power [20]. In summary, if following a voltage disturbance, the PV power increases, the disturbance direction is maintained. If not, it is reversed to resume convergence to the new MPP. The implementation steps of the P & O technique are illustrated in **Figure 3**.

3.2. Hill-climbing method

The hill-climbing method [16, 21] consists in moving the operating point along the characteristic $I = f(V)$ in the direction in which the instantaneous power PPV increases. For this, the disturbance is applied for the duty cycle D of the converter. The search stops theoretically until the operating power oscillates at the MPP [22, 23]. The flow diagram of this method is illustrated in **Figure 4**.

3.3. Incremental conductance method

To find the MPP, this other technique is based on the knowledge of the GPV conductance variation and the consequences on the position of the operating point with respect to a PPM [24, 25]. Thus, the conductance of the photovoltaic module is defined by the ratio between the current and the voltage of the GPV as indicated below:

The conductance G of the PV circuit is:

$$G = I_{pv} / V_{pv} \quad (4)$$

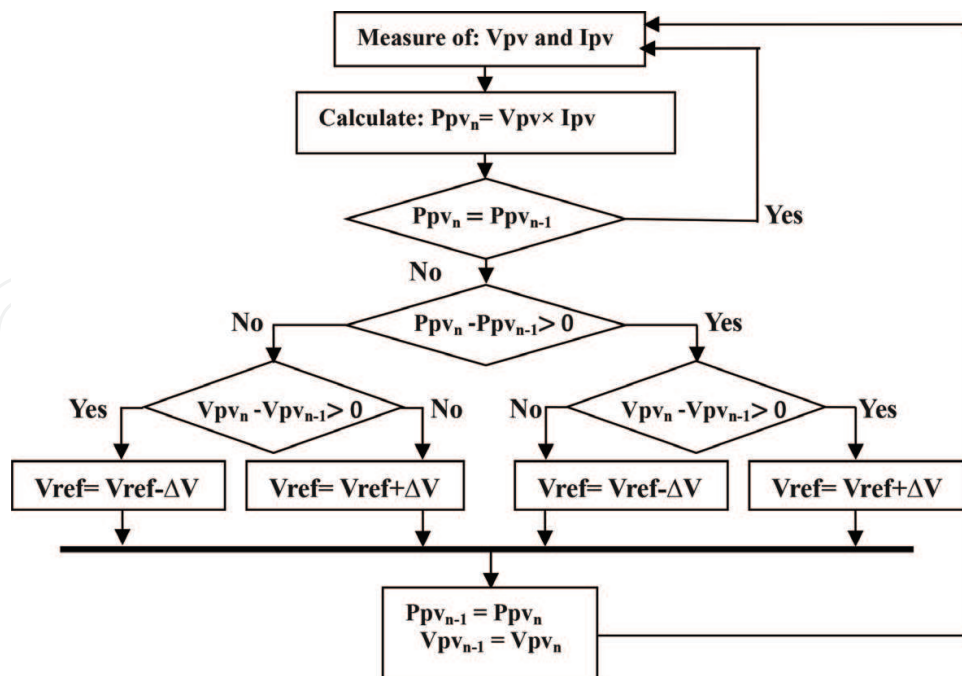


Figure 3. Algorithm of an MPPT command based on the P&O method.

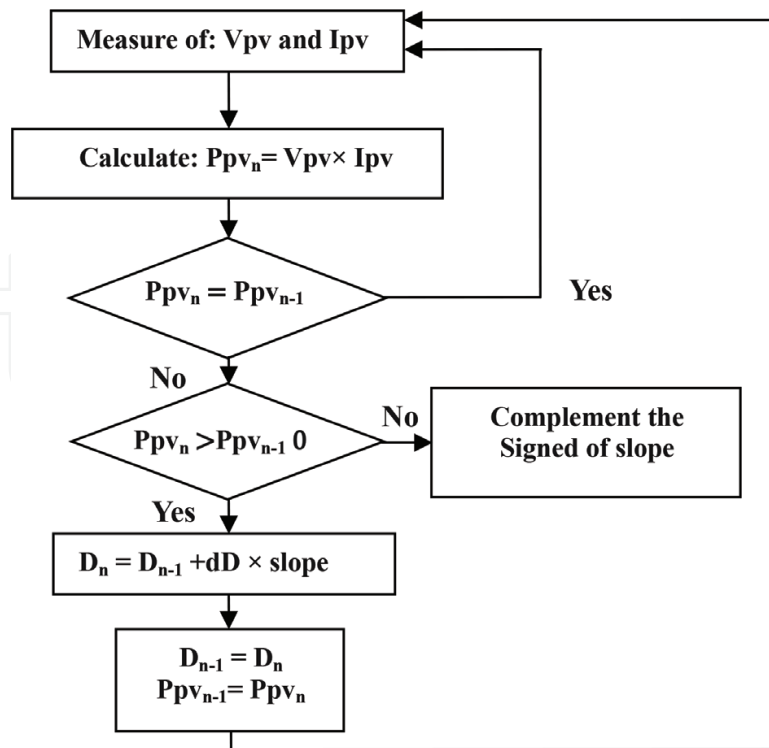


Figure 4. Algorithm of an MPPT command based on the hill-climbing method.

Moreover, an elementary variation (increment) conductance can be defined by:

$$dG = dI_{pv} / dV_{pv} \quad (5)$$

Figure 5 shows the position of the operating point on the power characteristic of the PV generator.

The equation of PV panel power is:

$$P_{pv} = V_{pv} \times I_{pv} \quad (6)$$

$$\begin{cases} \frac{dP_{pv}}{dV_{pv}} = \frac{d(V_{pv} \times dI_{pv})}{dV_{pv}} \\ \frac{dP_{pv}}{dV_{pv}} = I_{pv} + V_{pv} \frac{dI_{pv}}{dV_{pv}} \\ \frac{1}{dV_{pv}} \times \frac{dP_{pv}}{dV_{pv}} = \frac{I_{pv}}{V_{pv}} + \frac{dI_{pv}}{dV_{pv}} \end{cases} \quad (7)$$

where:

$$P_{pv} = P_{pv_n} - P_{pv_{n-1}}, \quad dV_{pv} = V_{pv_n} - V_{pv_{n-1}} \quad \text{and} \quad dI_{pv} = I_{pv_n} - I_{pv_{n-1}} \quad (8)$$

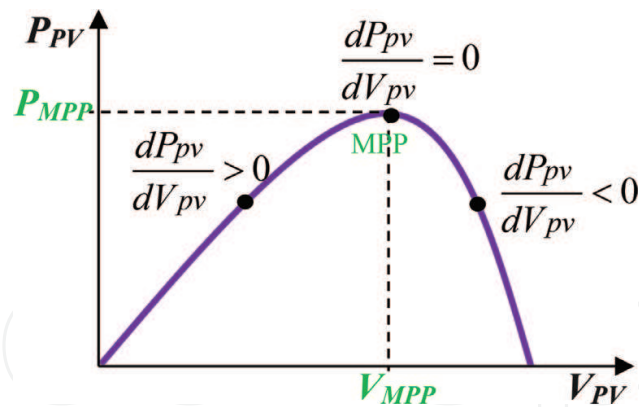


Figure 5. PV power characteristic for different operating points.

On the other hand, the evolution of the power of the module (P_{PV}) with respect to the voltage (V_{PV}) gives the position of the operating point relative to the PPM. When the power derivative is zero, it means that it is on the PPM, if it is positive the operating point is to the left of the maximum, when it is negative, it is to the right of the MPP [23]. Figure 5 allows to write the following conditions:

$$dP_{pv}/dV_{pv} = 0 \quad \text{At the MPP.} \quad (9)$$

$$dP_{pv}/dV_{pv} > 0 \quad (10)$$

$$dP_{pv}/dV_{pv} < 0 \quad (11)$$

4. Design and realization of the digital MPPT algorithm

At this stage of the research, we will explain the design steps and the realization of the electronic card based on the MPPT algorithms integrated in a microcontroller (μC) PIC. This digital MPPT control based μC has several advantages over analog MPPT control [26, 27]. Our control board contains three important blocks: power block, power supply, and control block.

4.1. Dimensioning of the power block

The control block consists of two essential parts: the measuring circuit is used to read the voltage and current of our photovoltaic panel at the input of the control unit. The second part, which is actually the brain of this block is formed by a microcontroller PIC 16F877A, to program the various proposed MPPT algorithms, and sends the control signal (the duty cycle) of the chopper to the power block, after isolation and amplification.

- **Tensions measurement:** So that the microcontroller can read the voltage of the photovoltaic panel, we must perform the operation of transforming a voltage of 0–22 V into a voltage of 0–5 V.

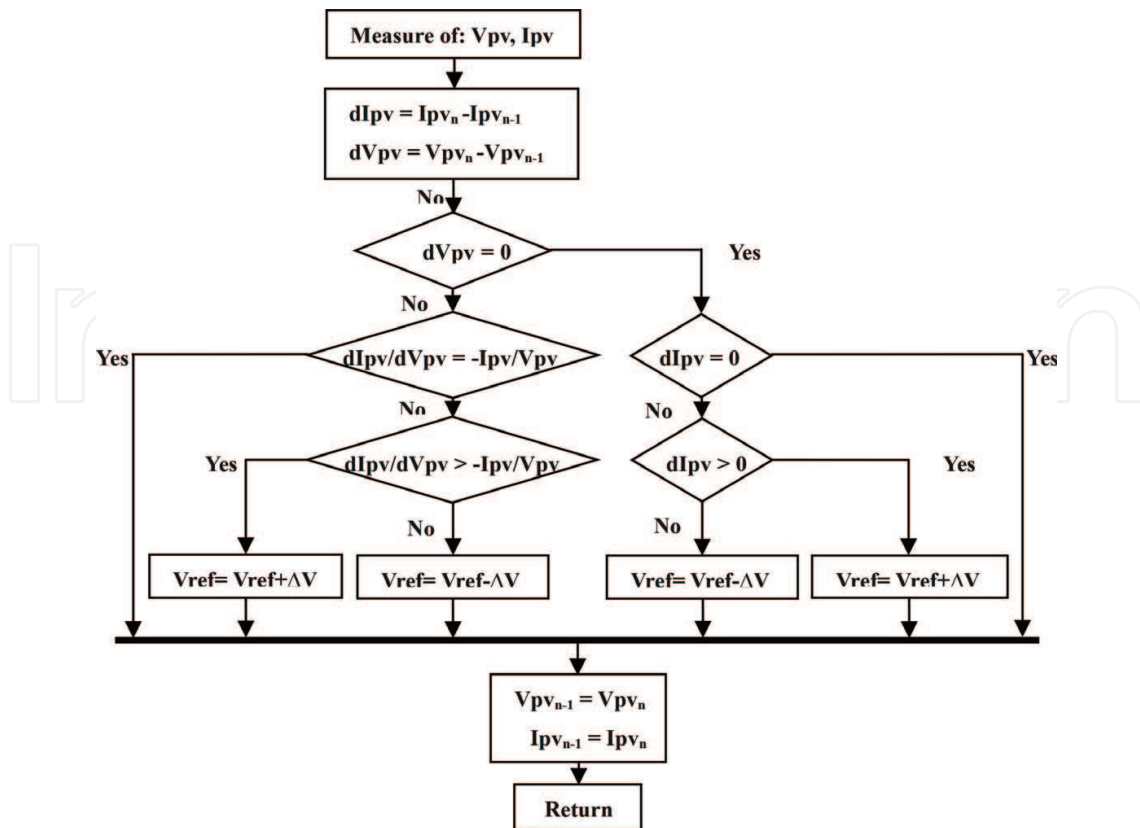


Figure 6. MPPT control algorithm based on IncCond [10].

It is therefore with a simple voltage divider bridge that we perform this operation as show in **Figure 10**. The voltage input to PIC (ΔV_{PIC}) will be connected to pin AN1 of port A configured as input:

Calculation of the resistances:

We choose $V_{PV} = 22(\text{Volts})$ (photovoltaic panel open circuit voltage) and $V_{PIC} = 5(\text{Volt})$ as the maximum input value to the microcontroller:

$$V_{PIC} = \left(\frac{R_2}{R_1 + R_2} \right) \cdot V_{PV} \Rightarrow \frac{V_{PIC}}{V_{PV}} = \left(\frac{R_2}{R_1 + R_2} \right) \quad (12)$$

Digital application: $\frac{5}{22} = \left(\frac{R_2}{R_1 + R_2} \right)$.

For: $R_2=1 \text{ (K}\Omega) \iff R_1=3.4 \text{ (K}\Omega)$.

- **Current measurement**

For the measurement of the current derived from the PV module, an inverter amplifier based on an operational amplifier TL082 was chosen. This configuration allowed us to read the value of the current of the panel, with the mass chosen on the side of the load.

The following formulas determine the parameters of this circuit:

$$V_S = \left(-\frac{R_4}{R_3} \right) \cdot V_E \quad \text{With } (V_E = R_{sh} \cdot I_{PV}) \quad (13)$$

So output voltage:

$$V_S = (R_{sh} \cdot I_{PV}) \cdot \left(\frac{R_4}{R_3} \right) \quad (14)$$

With:

$R_{sh} = 0,1(\Omega)$, V_S : output voltage, V_E : Tension d'entrée input voltage.

4.2. The power block

A Buck converter, or chopper, is a switching power supply that converts a DC voltage into another DC voltage of lower value. Using this converter, the DC input voltage, which is for example generated by the photovoltaic generator (GPV) as shown in **Figure 7**, can be lowered. This serial converter can be used as a source-load adapter, when the direct-coupled operating point is to the left of the MPP. For points to the right of the MPP point, the boost converter is more efficient [28].

It consists of a DC-DC buck converter based on IGBT BUP 314, and ensuring the transfer of all of the power extracted from the solar panel to a resistive load.

If switch **S1** is turned on, diode **D** is reverse biased and a circuit current occurs, but does not pass through this diode (**Figure 8**).

The current i_L does not increase immediately, but increases with a rate imposed by inductance **L** [28]:

$$\frac{di_L}{dt} = \frac{V_{PV} - V_{ch}}{L} \quad (15)$$

Meantime, the inductor stores the energy in a magnetic form. If switch **S1** is deactivated after $t = t_1$, the load is separated from the source (system supplied). The current is however maintained

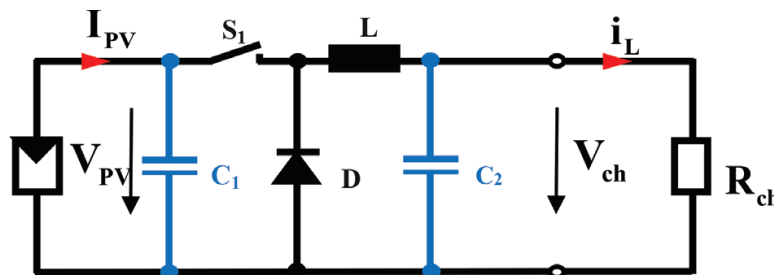


Figure 7. Diagram of the electrical circuit of a Buck converter.

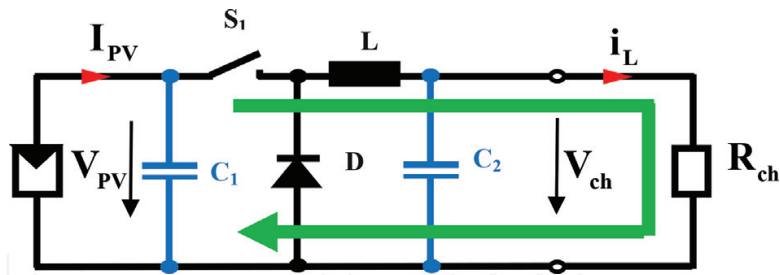


Figure 8. Convertisseur buck Durant l'état on.

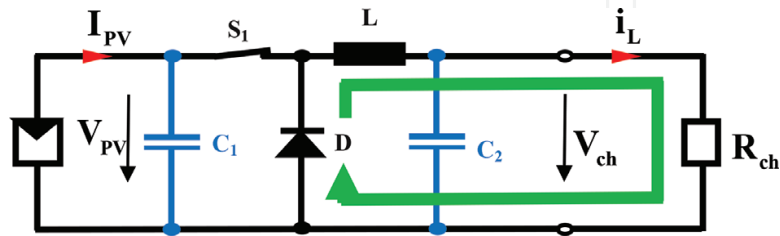


Figure 9. Convertisseur buck Durant l'état off.



Figure 10. PV module employed in the experiment.

by the energy stored in the inductor L and flows by means of the freewheeling diode (Figure 9). By neglecting the voltage drop across the diode, the current falls, however, because of the following equation:

$$\frac{di_L}{dt} = \frac{-V_{ch}}{L} \quad (16)$$

Capacitor C_1 is used to support the supply voltage (V_{pv}). In principle, the switch S_1 is activated and deactivated with a switching frequency f .

The 80 Watt PV panel used in this study is shown in Figure 10.

We operate our serial converter in continuous conduction mode (CCM) and the parameters of this circuit are $C_1 = 2200 \mu F$, $C_2 = 200 \mu F$ and $L = 600 \mu H$. This value of 'L' has been chosen so that the converter operates in TLC according to the following equation [29, 30]:

$$L > \frac{V_{pv}}{4 \times dIL \times f} \tag{17}$$

4.3. The energy block

The operation of our control circuit requires a power supply at three voltage levels. For this, we realized four power supplies based on a voltage regulator:

- The LM 7805 voltage regulator to supply the microcontroller with a fixed voltage equal to 5 V.
- The two LM 7815 and LM 7915 voltage regulators to provide power required current sensor (−15 V and +15 V), based on an operational amplifier the TL082.
- A second LM 7815 regulator to power the 4 N25 optocoupler with +15 V voltage. The latter will serve as a driver for the power switch, to ensure the galvanic isolation between the power block and the control block.

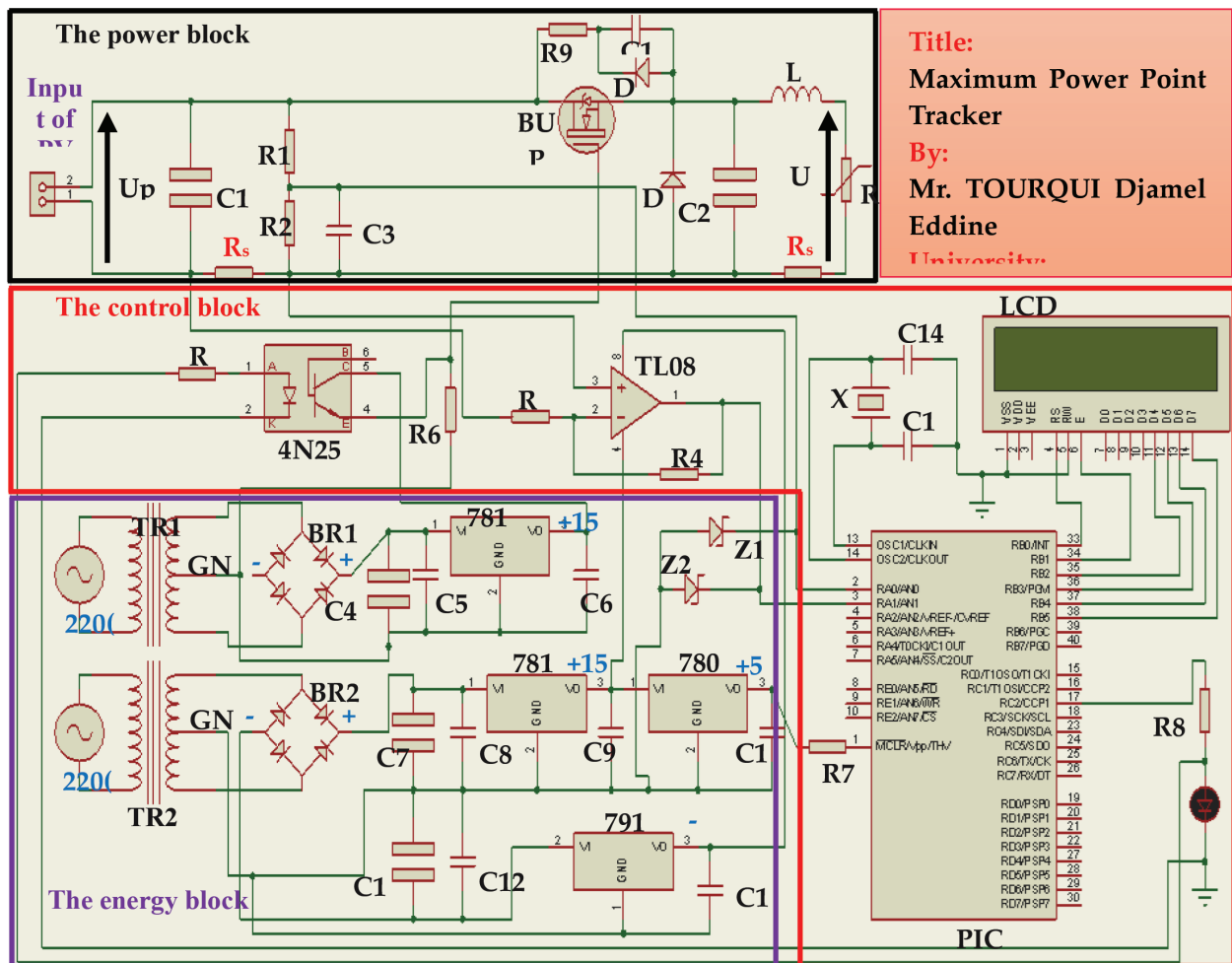


Figure 11. Electrical diagram of the prototype realized.

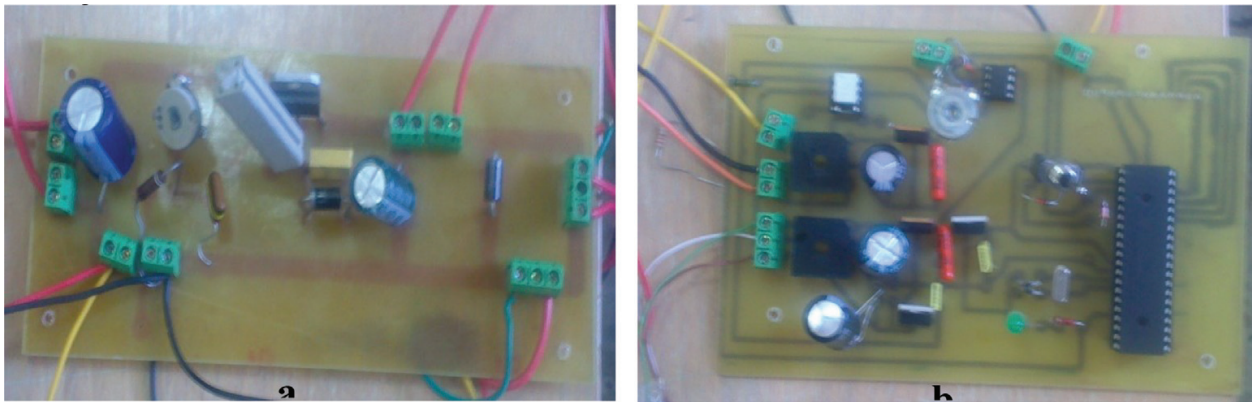


Figure 12. Practical realization of the electronic cards.

The diagram of **Figure 11**, representing the prototype to be produced, was made under the Proteus PCB design software designed by 'Labcenter Electronics', which makes it possible to draw electronic diagrams, to simulate them and to produce the corresponding printed circuit.

Figure 12a and **b** represents the prototype, which has been realized practically for the digital MPPT control.

5. Results obtained from the MPPT control

In this part, we present the experimental results of the three numerical MPPT algorithms: Perturbed & Observed, Hill-Climbing, and Incremental Conductance, tested on a resistive load ($R_m = 3.1 \text{ } (\Omega)$), which is lower than the load of the maximum power point (MPP) within three (03) clear days. These experiments have been done under the following operating conditions: (1) direct coupling of the load with the photovoltaic panel without MPPT control, (2) using digital MPPT control (DMPPT), (3) by manual MPPT until finding a position to the MPP (manual variation of the load value).

As a result of characteristic $I = f(V)$, we have found that the power generated (P) by the solar panel is related to the intensity of the radiation E and the temperature T_{amb} . We will take the measurements of: E , T_{amb} , P and efficiency of control η for each of the three MPPT algorithms studied (Perturb and Observe, Hill-climbing and Incremental Conductance). **Tables 1–3** illustrate the results obtained from the different experiments studied.

The histograms of **Figures 13–15** for these three methods show the difference between the power in the case of direct coupling and the power recovered when applying digital MPPT control that it is compared by the maximum power point search method manually.

Figure 16 illustrates current and voltage (U_{pv} , I_{pv}) of the photovoltaic generator, current and voltage of the resistive load (U_{ch} , I_{ch}) for direct coupling and MPPT cases based on the P & O technique.

Time (hh:mm)	P for direct coupling (watt)	P for DMPPT (watt)	P in MPP (watt)	η (%)	E (watt/m ²)	Tamb (°C)
10:10	18	43	43	100	672	35.6
11:20	25	54	54	100	809	39.3
15:45	12	40	41	97.5	546	39.5
16:11	9	35	35	100	466	35.5
16:30	6	31	32	96.8	404	34.5

Table 1. Experimental values identified by the P&O control

Time (hh:mm)	P for direct coupling (watt)	P for DMPPT (watt)	P in MPP (watt)	η (%)	E (watt/m ²)	Tamb (°C)
09:58	14	39	42	92.8	547	41.5
10:55	18	48	49	97.9	697	44.3
11:27	22	52	52	100	749	46.5
12:10	22	52	53	98.1	774	45.5
13:50	20	47	47	100	686	45.5

Table 2. Experimental values identified by hill-climbing control

Time (hh:mm)	P for direct coupling (watt)	P for DMPPT (watt)	P in MPP (watt)	η (%)	E (watt/m ²)	Tamb (°C)
13:05	27	54	54	100	774	39.3
13:55	22	53	53	100	835	41
14:25	21.5	54	54	100	772	42
14:46	18	50	50	100	715	45.5
15:12	15	45	45.5	98.9	645	45.5

Table 3. Experimental values identified by IncCond control

The duty cycle of the converter in the case of the P & O algorithm is illustrated in **Figure 17**.

The results of current and voltage of PV panel and the load obtained by Hill-climbing algorithm as shown in **Figure 18**. **Figure 19** explains the duty cycle that controlled the DC-DC converter.

Finally, the same experiment is performed using IncCond control and the results shown in **Figure 20**. **Figure 21** shows the duty cycle generated by the IncCond algorithm.

- **Interpretation and discussion of the results**

The results obtained previously in the power tables and histograms clearly show the efficiency of the electronic control card filled for different control algorithms used. The energy extracted from the solar panel using the digital MPPT technique is very large compared to the direct

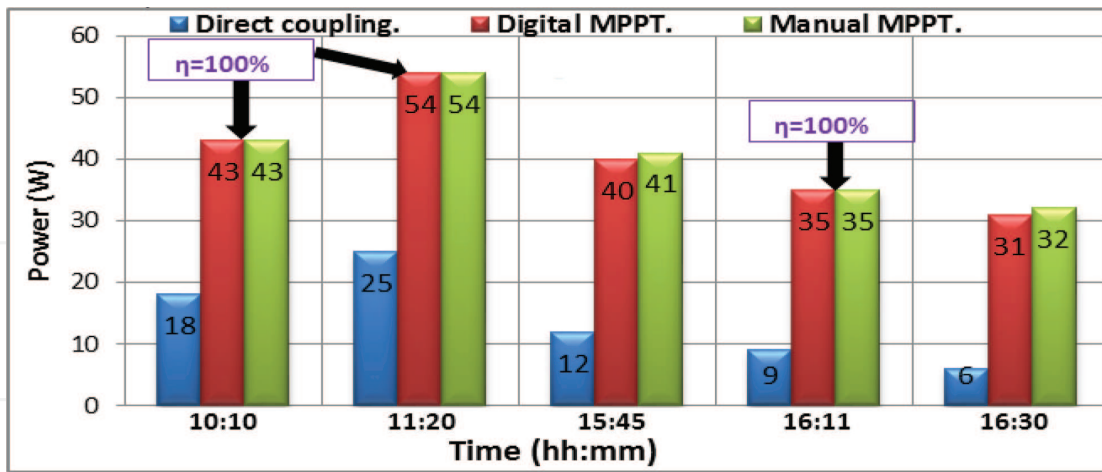


Figure 13. Histogram of powers to P&O algorithm.

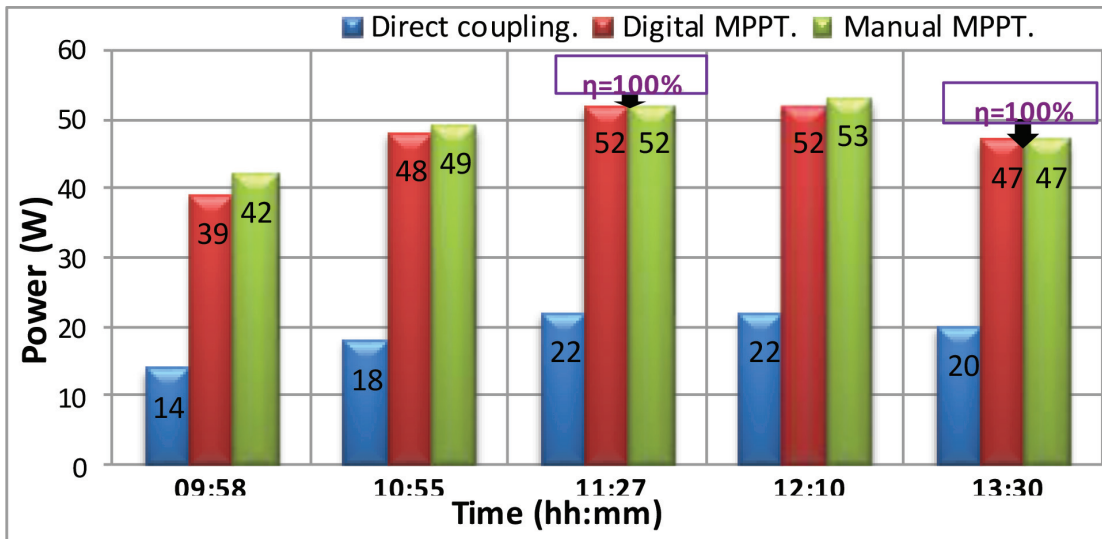


Figure 14. Histogram of powers to hill-climbing algorithm.

charge connection method with the panel. Therefore, in the case of a direct connection between the generator and the load is unlikely to place the PV system at its maximum power point PPM. However, the digital MPPT technique can automatically find the operating voltage of the PV panel that corresponds to the PPM. However, comparing the results obtained by the three algorithms shows the Incremental Conductance technique is the most accurate and closest to the MPP compared to the other two methods.

In addition, the results clearly show the effectiveness of the tracking system (η) which in many cases reaches 100%. This efficiency represents the ratio between the maximum power obtained manually and the other using the MPPT command as indicated in the following equation:

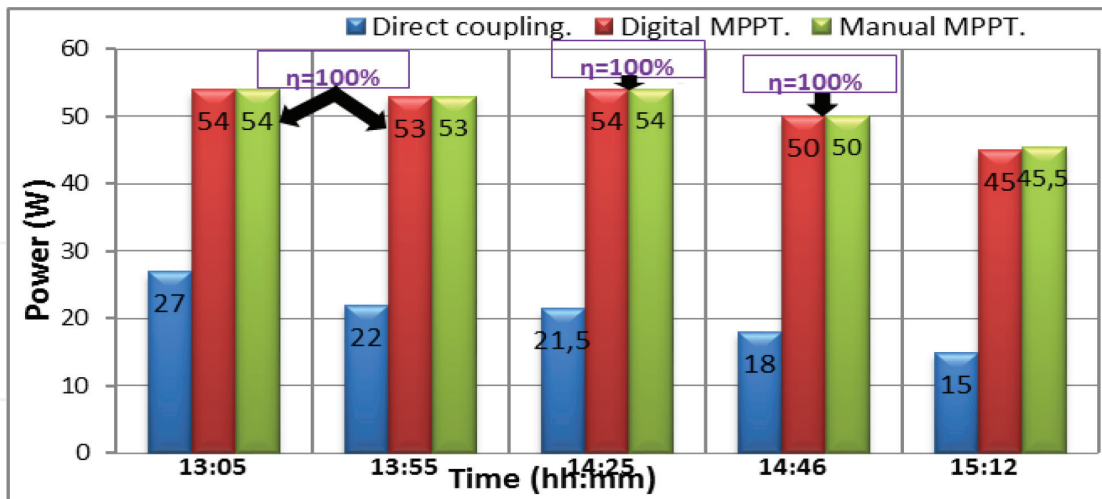


Figure 15. Histogram of powers to incremental conductance algorithm.

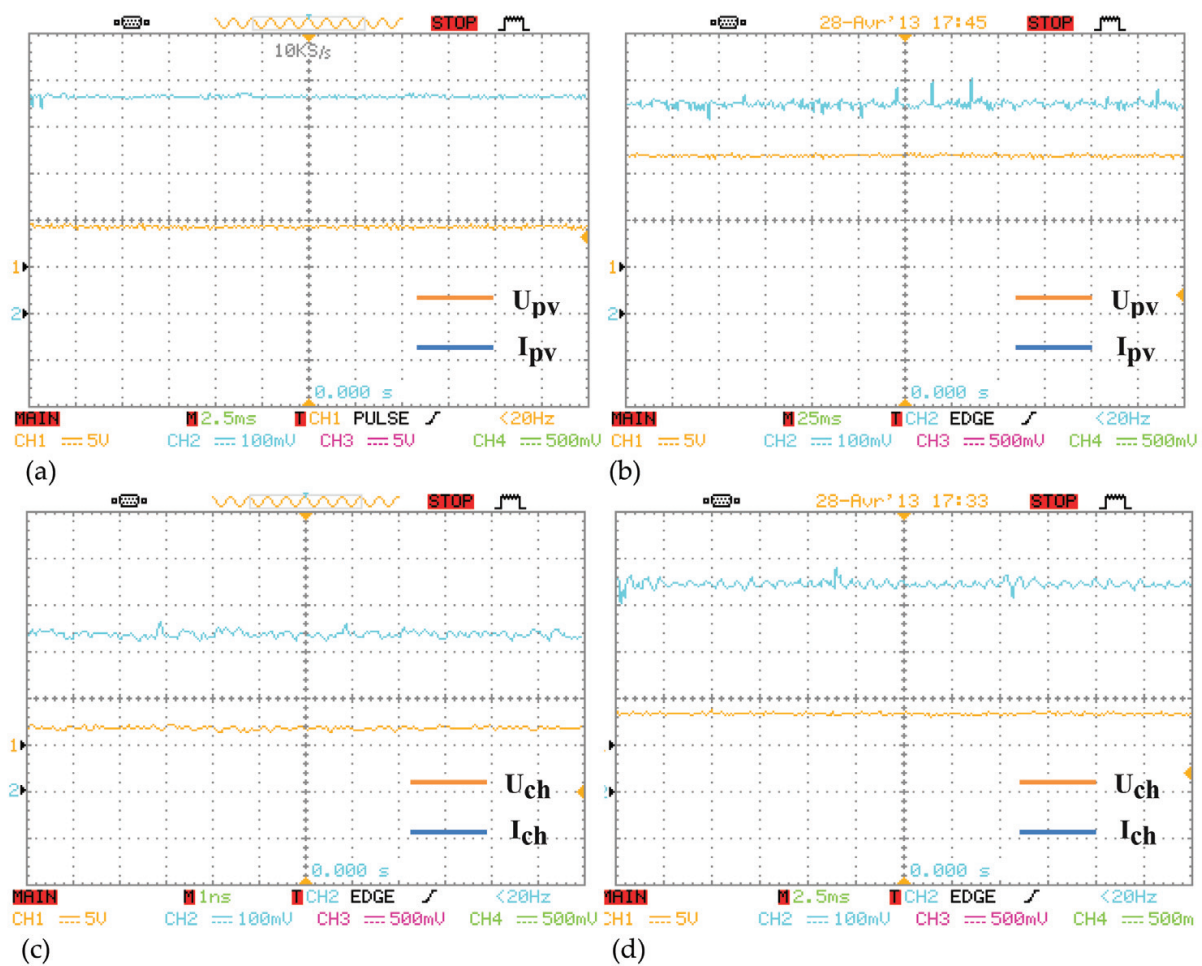


Figure 16. Current and voltage of the photovoltaic generator and the load. (a) (U_{pv} , I_{pv}) using direct coupling, (b) (U_{pv} , I_{pv}) using digital MPPT control, (c) (U_{ch} , I_{ch}) using direct coupling, (d) (U_{ch} , I_{ch}) using digital MPPT control.

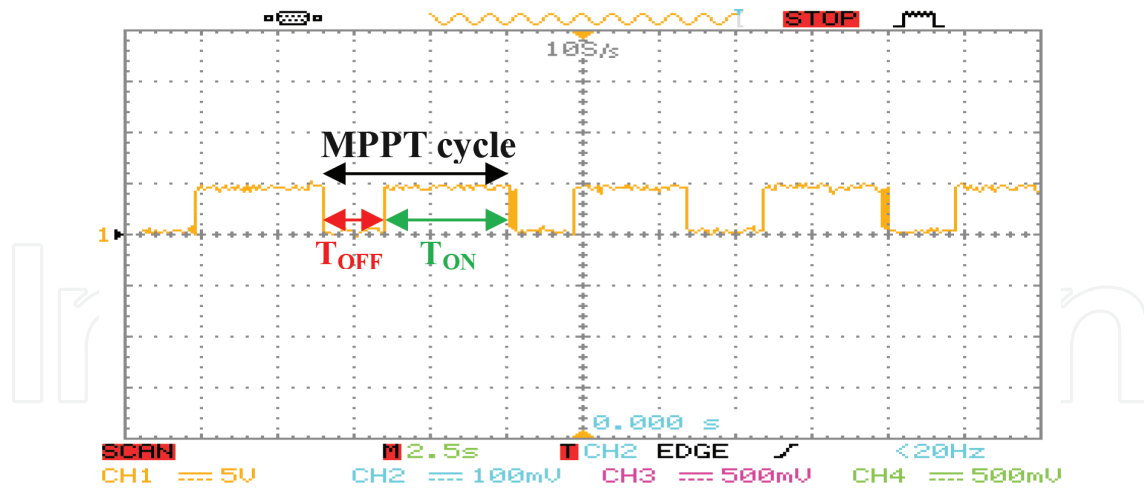


Figure 17. The duty cycle of the P&O algorithm.

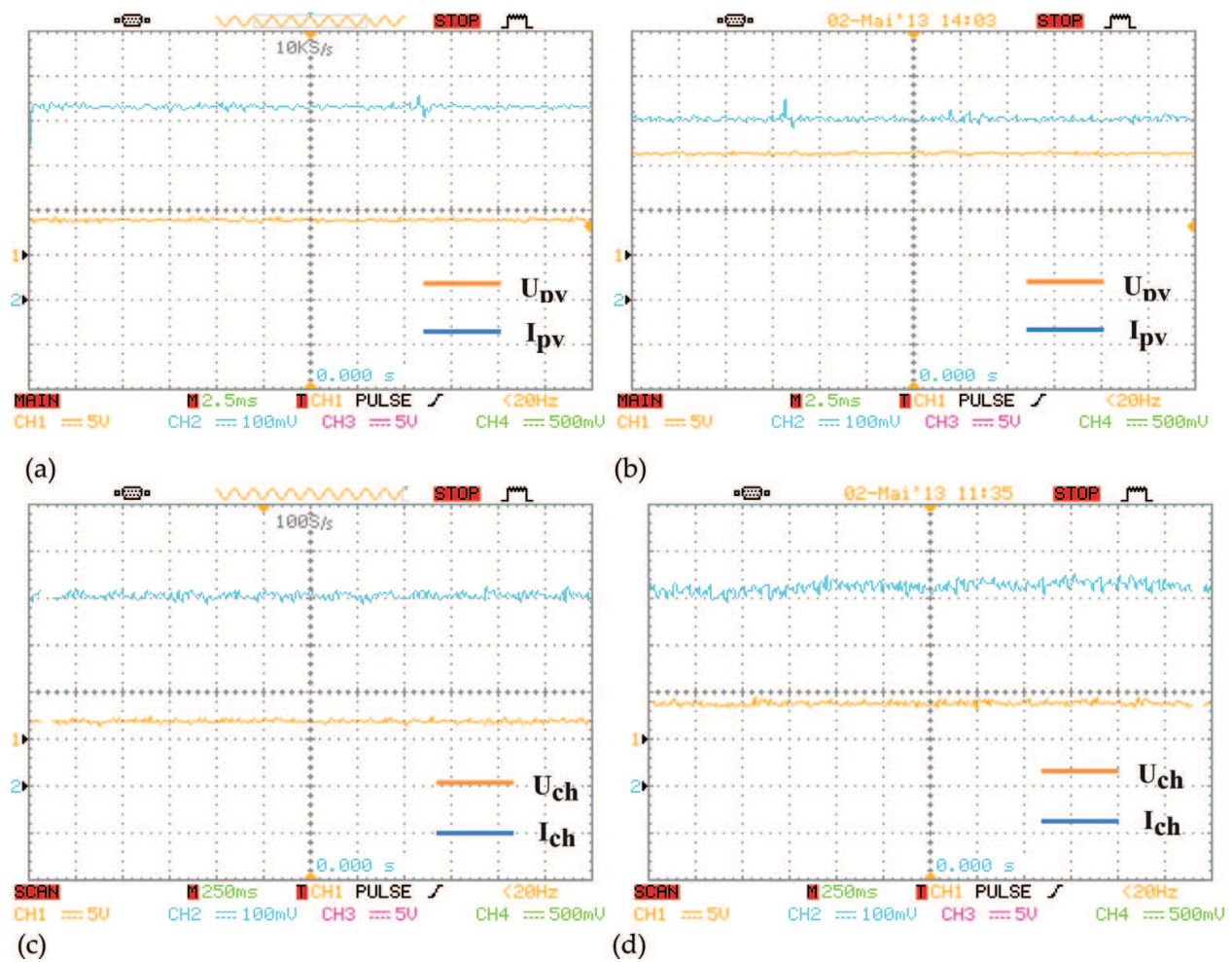


Figure 18. Current and voltage of the photovoltaic generator and the load. (a) (U_{pv} , I_{pv}) using direct coupling, (b) (U_{pv} , I_{pv}) using digital MPPT control, (c) (U_{ch} , I_{ch}) using direct coupling, (d) (U_{ch} , I_{ch}) using digital MPPT control.

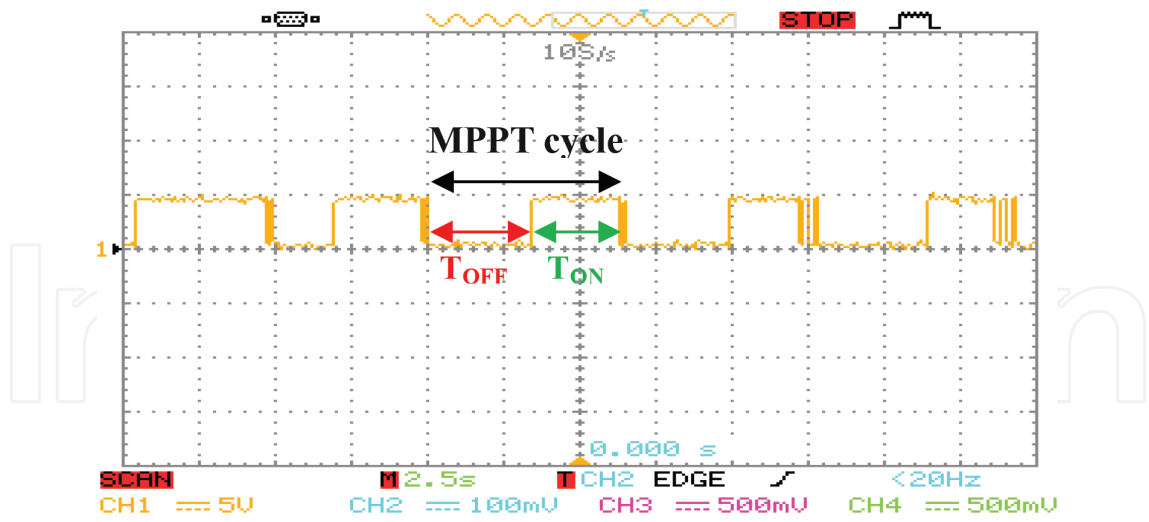


Figure 19. The duty cycle of the hill-climbing algorithm.

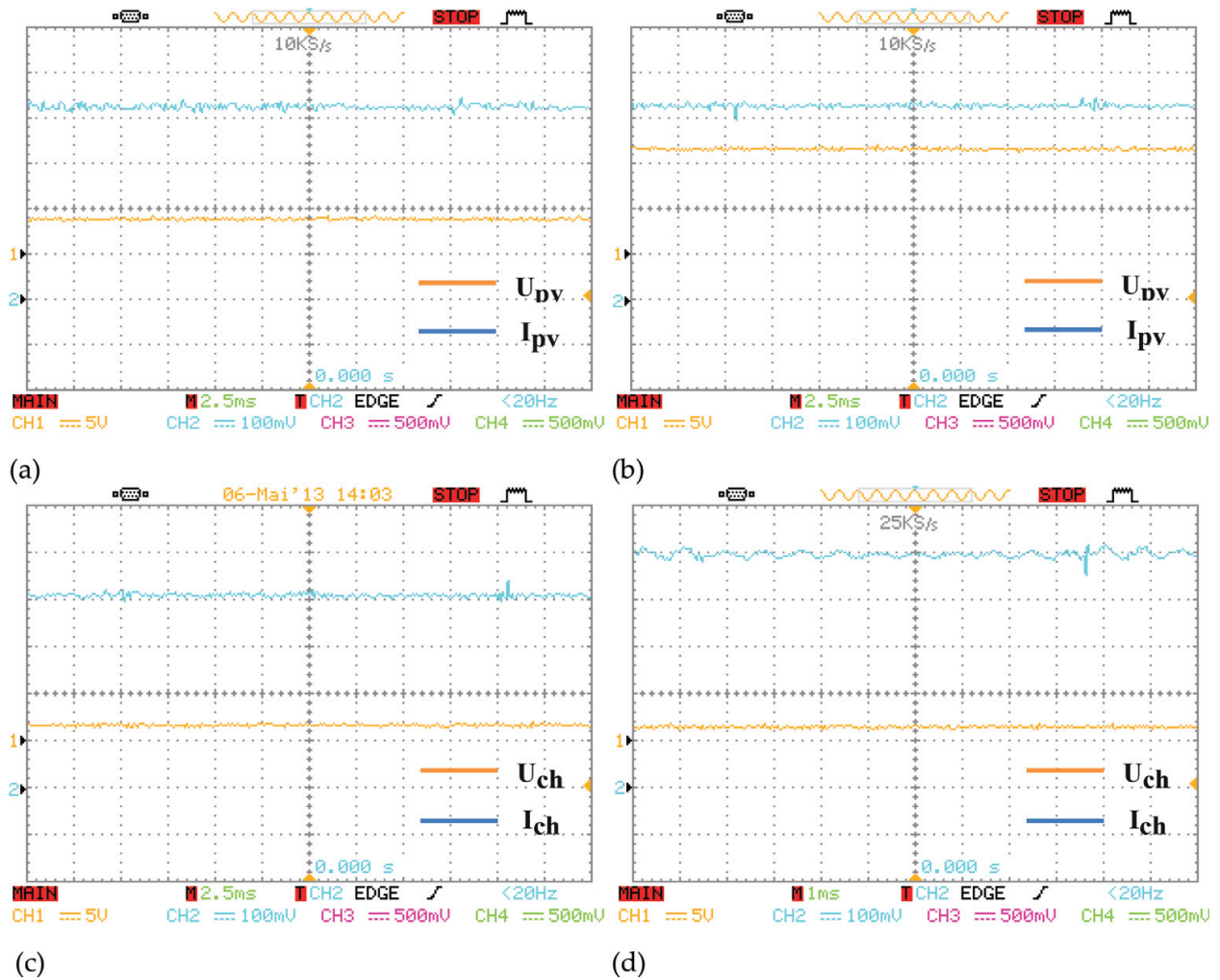


Figure 20. Current and voltage of the photovoltaic generator and the load. (a) (U_{pv} , I_{pv}) using direct coupling, (b) (U_{pv} , I_{pv}) using digital MPPT control, (c): (U_{ch} , I_{ch}) using direct coupling, (d) (U_{ch} , I_{ch}) using digital MPPT control.

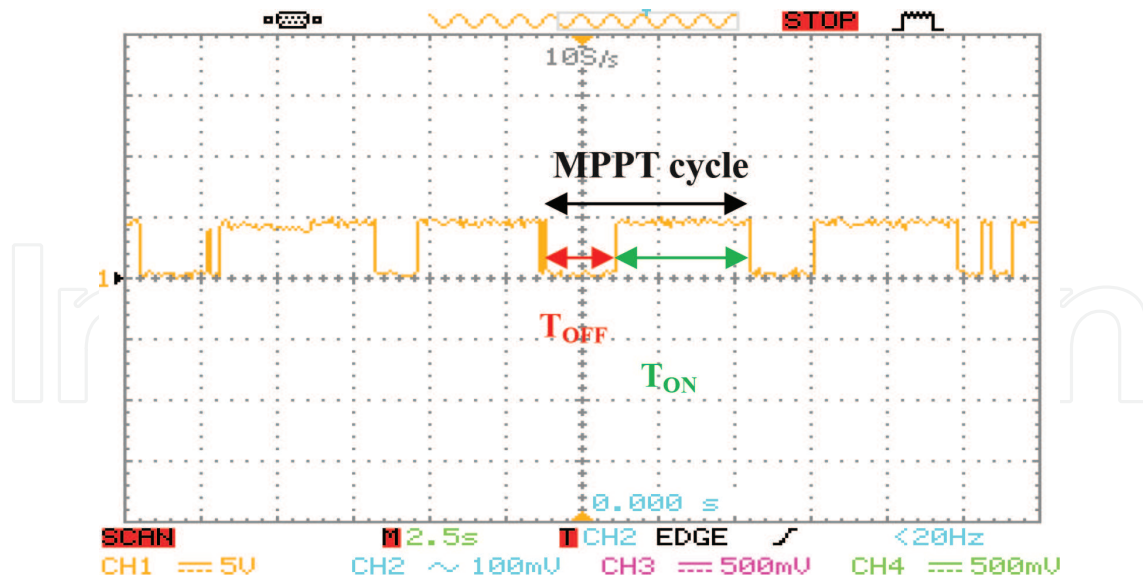


Figure 21. The duty cycle of the incremental conductance algorithm.

$$\eta(\%) = \frac{P_{DMPPT}}{P_{MPP}} \times 100 \quad (18)$$

where P_{DMPPT} represent the power reached by using the proposed of DMPPT controller and P_{MPP} is the expected maximum power output in the MPP.

Figures 16, 18 and 20 show that the chopper operates as a voltage step-down, with a voltage of the photovoltaic module stabilizes at $V_{pv} = 14.5$ (V). For the current of the load, it is found that the current is in continuous conduction, with a ripple of 2 kHz.

Finally, because of the integration of the PWM control signal into PIC, the duty cycle signal frequency generated by the MPPT command (Figures 18, 20 and 21) is of the order of 2 kHz. If the desired maximum power point voltage (V_{MPP}) is higher than the measured panel voltage (V_{pv}), the duty cycle must be incremented; it must be decreased according to the control technique used. This ratio is adjusted in real time, with the meteorological variations (E and T_{amb}), and this to position itself on the optimum point.

6. Conclusion and future action

The paper presented a simplified design and implementation of impedance matching stage using a DC-DC buck converter supplying a resistive load controlled by one low cost microcontroller. This circuit allows the acquisition and processing of measured current and voltage signals and generates the appropriate control signals for controlling the switching of the power unit designed primarily around the buck converter. Three popular MPPT algorithms for extracting the maximum power of the photovoltaic panel namely P&O, Hill-Climbing and IncCond have been considered.

MPPT control has led to improved speed of response, a better MPP search accuracy and good control in the presence of perturbations such as sudden variations of the illumination and the temperature.

This work enables us to increase the cost-effectiveness of solar systems as well as reduce the cost which were imported from abroad and the worldwide costly in terms of our scientific laboratory or sector level using this energy in sustainable development agriculture deployed locally as photovoltaic pumping, irrigation and domestic use.

In the future, experiment of these prototypes on other PV installations (like the PV pumping which is available in our laboratory) will be presented in future works.

Author details

Djamel Eddine Tourqui^{1*}, Achour Betka², Atallah Smaili³ and Tayeb Allaoui³

*Address all correspondence to: tourqui.djamel@gmail.com

1 Morsli Abdellah University Center of Tipaza, Algeria

2 Mohamed Khider University, Biskra, Algeria

3 Ibn Khaldoun University, Tiaret, Algeria

References

- [1] Mellit A, Massi PA. Performance prediction of 20kWp grid-connected photovoltaic plant at Trieste (Italy) using artificial neural network. *Energy Conversion and Management*. 2010;**51**:2431-2441
- [2] Parida B, Iniyamb S, Goicc R. A review of solar photovoltaic technologies. *Renewable and Sustainable Energy Reviews*. 2011;**15**:1625-1636
- [3] Mellit A, Kalogirou SA, Hontoria L, Shaari S. Artificial intelligence techniques for sizing photovoltaic systems: A review. *Renewable and Sustainable Energy Reviews*. 2009;**13**:406-419
- [4] Shraif MF. Optimisation et Mesure de Chaîne de Conversion d'Énergie Photovoltaïque en Énergie Électrique [Phd]. Toulouse, France: Paul Sabatier University; 2002
- [5] Orabi M, Hilmy F, Shawky A, Jaber AAQ, Hasaneen E, Gomaa E. On-chip integrated power management MPPT controller utilizing cell-level architecture for PV solar system. *Solar Energy*. 2015;**117**:10-28
- [6] Sivakumar P, Abdullah AK, Yogeshraj K, Arutchelvi M. Analysis and enhancement of PV efficiency with incremental conductance MPPT technique under non-linear loading conditions. *Renewable Energy*. 2015;**81**:543-550

- [7] Anaya-Lara O, Jenkins N, Ekanayake J, Cartwright P, Hughes M. Wind Energy Generation, Modelling and Control. John Wiley & Sons; 2009. ISBN: 978-0-470 71433-1
- [8] ESRAM T, Chapman PL. Comparison of photovoltaic array maximum power point tracking techniques. IEEE Transactions on Energy Conversion. 2007;**22**:439-449
- [9] De Brito MAG, Galotto L, Sampaio LP, de Azevedo EMG. Evaluation of the main MPPT techniques for photovoltaic applications. IEEE Transactions on Industrial Electronics. 2013;**60**:1156-1167
- [10] Learreta AB. Réalisation de commandes MPPT numériques. Report. Tarragona, Spain: Rovira i Virgili University; 2006
- [11] Sharaf Eldin SA, Abd-Elhady MS, Kandil HA. Feasibility of solar tracking systems for PV panels in hot and cold regions. Renewable Energy. 2016;**85**:228-233
- [12] Ingegnoli A, Iannopollo A. A maximum power point tracking algorithm for stand-alone photovoltaic systems controlled by low computational power devices. In: 15th IEEE 2010 Mediterranean Electro-Technical Conference; 26–28 April 2010. Valletta, Malta: IEEE. pp. 1522-1527
- [13] Villalva MG, Gazoli JR, Ernesto RF. Comprehensive approach to modeling and simulation of photovoltaic arrays. IEEE Transactions on Power Electronics. 2009;**24**:1198-1208
- [14] Nema P, Nema RK, Rangnekar S. A current and future state of art development of hybrid energy system using wind and PV-solar. Renewable and Sustainable Energy Reviews. 2009;**13**:2096-2103
- [15] Garcia A, Balenzategui JL. Estimation of photovoltaic module yearly temperature and performance based on nominal operation cell temperature. Renewable Energy. 2004;**29**: 1997-2010
- [16] Cabal C. Optimisation énergétique de l'étage d'adaptation électronique dédié à la conversion photovoltaïque [Phd]. Toulouse, France: Paul Sabatier III University; 2008
- [17] Hohm DP, Ropp ME. Comparative study of maximum power point tracking algorithms using an experimental programmable maximum power point tracking test bed. In: IEEE 2000 Photovoltaic Specialists Conference; 15-22 September 2000; Anchorage, Alaska, USA: IEEE. pp. 1699-1702
- [18] Femia N, Petrone G, Spagnuolo G, Vitelli M. Optimization of perturb and observe maximum power point tracking method. IEEE Transactions on Power Electronics. 2005;**20**:963-973
- [19] Sera D, Kerekes T, Teodorescu R, Blaabjerg F. Improved MPPT algorithms for rapidly changing environmental conditions. In: Power Electronics and Motion Control Conference 2006; 30 August-1 September 2006; Portoroz, SLOVENIA: IEEE. 2006. pp. 1614-1619
- [20] Onat N. Recent developments in maximum power point tracking technologies for photovoltaic systems. International Journal of Photoenergy. 2010;**2010**:11. Article ID 245316. DOI: 10.1155/2010/245316

- [21] Xiao W, Dunford WG. Evaluating maximum power point tracking performance by using artificial lights. In: IEEE 2004 Industrial Electronics Society; 2–6 November 2004. Busan, Korea: IEEE; 2004. pp. 2883-2887
- [22] Shimizu TH, Kimura OG. A novel high performance utility interactive photovoltaic inverter system. IEEE Transactions on Industrial Electronics. 2003;18:704-711
- [23] Nur AK, Chee WT. A comprehensive review of maximum power point tracking algorithms for photovoltaic system. Renewable and Sustainable Energy Reviews. 2014;37:585-598
- [24] Lee JH, Bae H, Cho BH. Advanced incremental conductance MPPT algorithm with a variable step size. In: Power Electronics and Motion Control Conference; 30 August-1 September 2006, 2006. Portoroz, SLOVENIA: IEEE. pp. 603-607
- [25] Kim TY, Ahn HG, Park SK, Lee YK. A novel maximum power point tracking control for photovoltaic power system under rapidly changing solar radiation. In: IEEE 2001 International Symposium on Industrial Electronics; 12–16 June 2001. Busan, Korea: IEEE; 2001. pp. 1011-1014
- [26] Oi A. Design and simulation of photovoltaic water pumping system [MSc]. California, USA: California Polytechnic State University; 2005
- [27] Pongratananukul N. Analysis and simulation tools for solar array power systems [Phd]. Florida, USA: Central Florida Orlando University; 2005
- [28] Luque A, Hegedus S. Handbook of Photovoltaic Science and Engineering. USA: John Wiley & Sons Ltd; 2003
- [29] Group 01gr509. Power Supply for the AAU Cubesat. Report. AALBORG University; 2001
- [30] Erickson RW. Fundamentals of Power Electronics. New York, NY: Chapman & Hall; 1997